Diverse Amine-Acid Coupling Reactions Modulate the Potency of BRD4 PROTACs

Andrew McGrath[1], Haiyan Huang[1], Jean-Francois Brazeau[2], Zirong Zhang[1†], Nadeem A. Vellore[2], Lu Zhu[3], Zhicai Shi[4], Jennifer D. Venable[2], Christine Gelin[2*], Tim Cernak[1,5*]

AUTHOR ADDRESS

[1]Department of Medicinal Chemistry, University of Michigan, Ann Arbor, Michigan 48104

[2]In-Silico Discovery, Therapeutics Discovery, Janssen Research & Development, LLC, 3210 Merryfield Row, La Jolla, California 92121, United States

[3]Discovery Technologies & Molecular Pharmacology, Therapeutics Discovery, Janssen Research & Development, LLC, Welsh & McKean Roads, Spring House, Pennsylvania 19477, United States

[4]Discovery Chemistry, Therapeutics Discovery, Janssen Research & Development, LLC, Welsh & McKean Roads, Spring House, Pennsylvania 19477, United States

[5]Department of Chemistry, University of Michigan, Ann Arbor, Michigan 48104

KEYWORDS (Word Style "BG_Keywords"). amine–acid couplings, PROTAC, protein degradation, high-throughput experimentation, reductive amination

ABSTRACT: *Protein degradation with proteolysis targeting chimeras (PROTACs) has emerged as a powerful therapeutic strategy. PROTACs are heterobifunctional molecules consisting of a target-binding moiety, a linker and an E3 ligase-binding moiety that are commonly linked together using amide bonds. Although experimentally facile, this bond choice may impart sub-optimal drug properties to the overall PROTAC molecule. Here, we show that a suite of BRD4 PROTAC degraders were prepared via diverse amine-acid couplings beyond the amide bond, where the bromodomain inhibitor JQ1 carboxylic acid was used as the acid and the E3-derived (Cereblon or Von Hippel Lindau) partial PROTACs served as the amine. Four new amine–acid coupling reactions were developed to generate the ester, ketone, alkane, or amine bond connection using miniaturized high-throughput experimentation (HTE). Subtle reaction condition effects in nickel and platinum catalyzed couplings on complex molecule substrates were uncovered, and the toolbox of linkage methods to synthesize heterobifunctional degraders was expanded. Calculated physicochemical properties for these ten diversly linked PROTACs showed a wide range of lipophilicity, polar surface area, and hydrogen bonding characteristics. Ultimately, when these compounds were evaluated for BRD4 degradation, several of them showed improved efficacy. The ester, ketone, and alkane linked degraders outperform the classic amide-linked compound. This study highlights the impact that slight changes to the linkage between the protein of interest (POI) and E3 ligase binders can be used to modulate degradation and drug properties.*

The ability to covalently unite two molecules is critical to studies in proximity-induced pharmacology, medicinal chemistry, polymer chemistry, chemical biology, antibody-drug fusion and other diverse bioconjugation applications. Recently, the emergence of proteolysis targeting chimeras (PROTACs) as a powerful therapeutic modality has highlighted the role that the linker composition has not only on the activity, but also the bulk physicochemical properties of these protein degraders.[1–6] PROTACs are heterobifunctional ligands that contain a ligand to recruit an E3 ubiquitin ligase, a ligand to bind the protein of interest (POI), and a linker conjoining the two ligands, leading to event driven pharmacology that is catalytic and agnostic of receptor occupancy.[7] As such, PROTACs have a unique ability to eliminate "undruggable" protein targets. The explosion of interest in PROTACs has led to an extensive, commercially available toolkit of linker and E3 ligase binding building blocks, many of which terminate in an amine or carboxylic acid. The amide reaction is one of the most popular methods for linking two molecules together and has been broadly used in the development of PROTACs.[8,9] Other tactics include esterification[10], click chemistry,[11] S_NAr,[12] Buchwald–Hartwig coupling,[13] among other new methods.[14,15] Each of these methods represents a powerful way to unite the POI and E3

ligase pair, but often requires multi-step synthesis to install an alternative reactive functional group on one or both binders. Recently, we have shown that amines and carboxylic acids can be united in many ways beyond the amide connection, with each amine–acid coupling transformation imparting a distinct physicochemical footprint on the product.[16–21] Given that the linker moiety may affect degradation efficiency as well as absorption, distribution, metabolism and excretion (ADME) properties such as permeability of PROTACs,[22] we sought to explore new reactions that would expand access to diverse linkages between a POI and E3 ligase ligands, and examine the influence of the linker changes on the biological activity of certain final PROTACs.

Conventionally, when a primary amine and carboxylic acid are coupled together[23], the resultant amide motif bears one hydrogen bond donor (HBD) along with two hydrogen bond acceptors (HBA) and a neutral charge. In this manner, the transformation itself can be viewed as leaving a physicochemical footprint on the product. However, if the conditions used in the reaction are modified and an ester is produced instead, the HBD is removed from the product. It follows that the functional outcome of a molecule is dependent not only upon the building blocks used to create it but also the transformation used to unite these fragments which are intertwined with the selected reaction conditions. In this way, shifts in the composition and arrangement of atoms allow for a fine tuning of the property space accessible from just two building blocks by changing reaction conditions.[17] We have developed transformations that couple amines and acids into esters,[18,19] alkanes,[20,21] and ketones.[21] The application of complementary amine–acid coupling transformations to assemble PROTACs is particularly intriguing, considering the important role that the linker design itself may play on properties. Herein, we developed a suite of amine–acid PROTACs linking reactions that produced either an amide, ester, amine, alkane, or ketone linkage using the well-studied bromodomain inhibitor JQ1 **1** and cereblon (CRBN) binding pomalidomide derived amine **2** to yield derivatives **4**–**7** of the classic PROTAC dBET1 (**3**) (Figure 1a).[24] Our suite of heterobifunctional degraders, accessed from these two starting materials was expanded upon by applying the same transformations to a von Hippel-Lindau (VHL) targeting amine. The resultant compounds span a range of physicochemical and pharmacological properties.

Furthermore, when 80 possible transformations[16] were applied on **1** and a suite of commercially available CRBN recruiting amines *in silico*, a diverse property space emerged. The properties of these molecules, including molecular weight, LogP, formal charge, and polar surface area (PSA) (see Supporting Information/Github) were calculated and compared for the 80 possible transformations using a t-Distributed Stochastic Neighbor Embedding (tSNE) (Figure 1b). This analysis revealed the amide (purple) and amine (yellow) transformations in general occupy their own chemical space, suggesting these transformations impart a larger effect on the overall properties of the molecule. Comparatively, the ester (pink), alkane (red), and ketone (orange) overlap in chemical space, indicating these transformations exert a more nuanced effect on the property space

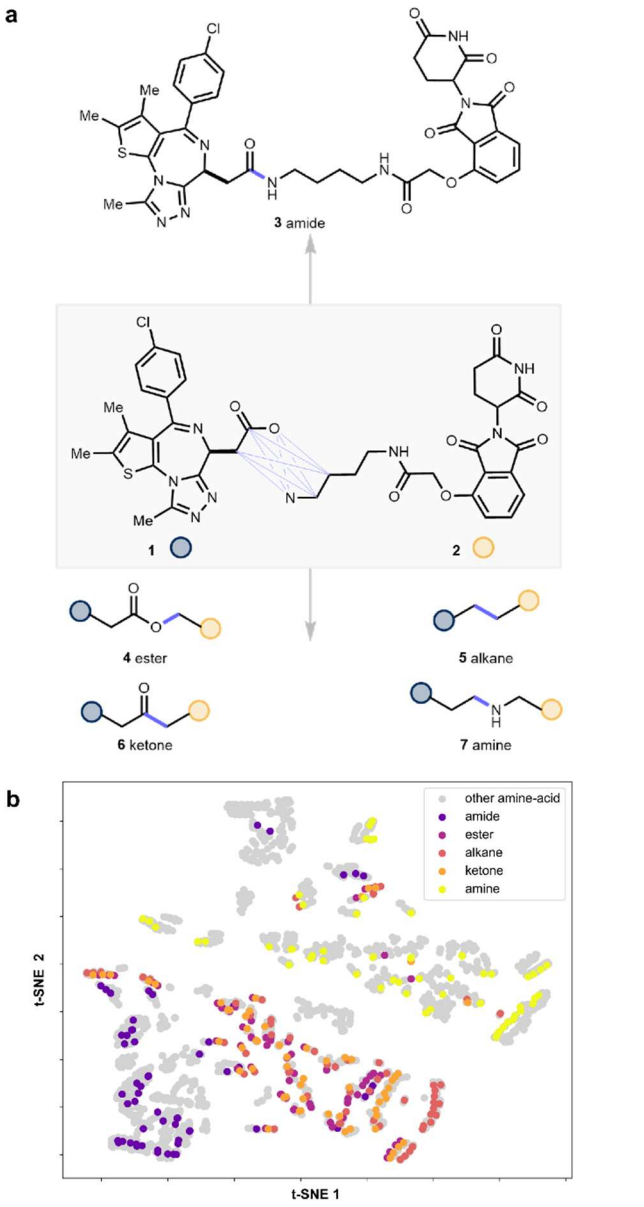

Figure 1. (a) Diverse amine–acid couplings on **1** and **2** can produce amide (**3**), ester (**4**), alkane (**5**), ketone (**6**), or amine (**7**), congeners. (b) These transformations and 75 others (ref. 16) are applied to **1** and a collection of commercially available amine-containing partial PROTACs (see Supporting Information) to give a chemical space, displayed as a t-distributed stochastic neighbor embedding (tSNE), with amide, ester, amine, alkane, ketone products highlighted in color.

occupied by the products. This is further exemplified by the incorporation of basic amines into the linker portion of the starting amine (c.f. orange dots in the yellow space). Notable inaccessible pockets (grey) of this space that remain include transformations that retain the carboxylic acid or incorporate rearrangements (See Supporting Information), representing synthetic methods that may be possible to investigate in the future. However, these four new transformations cover a breadth of space and offer new structure activity relationships from the same two building blocks.

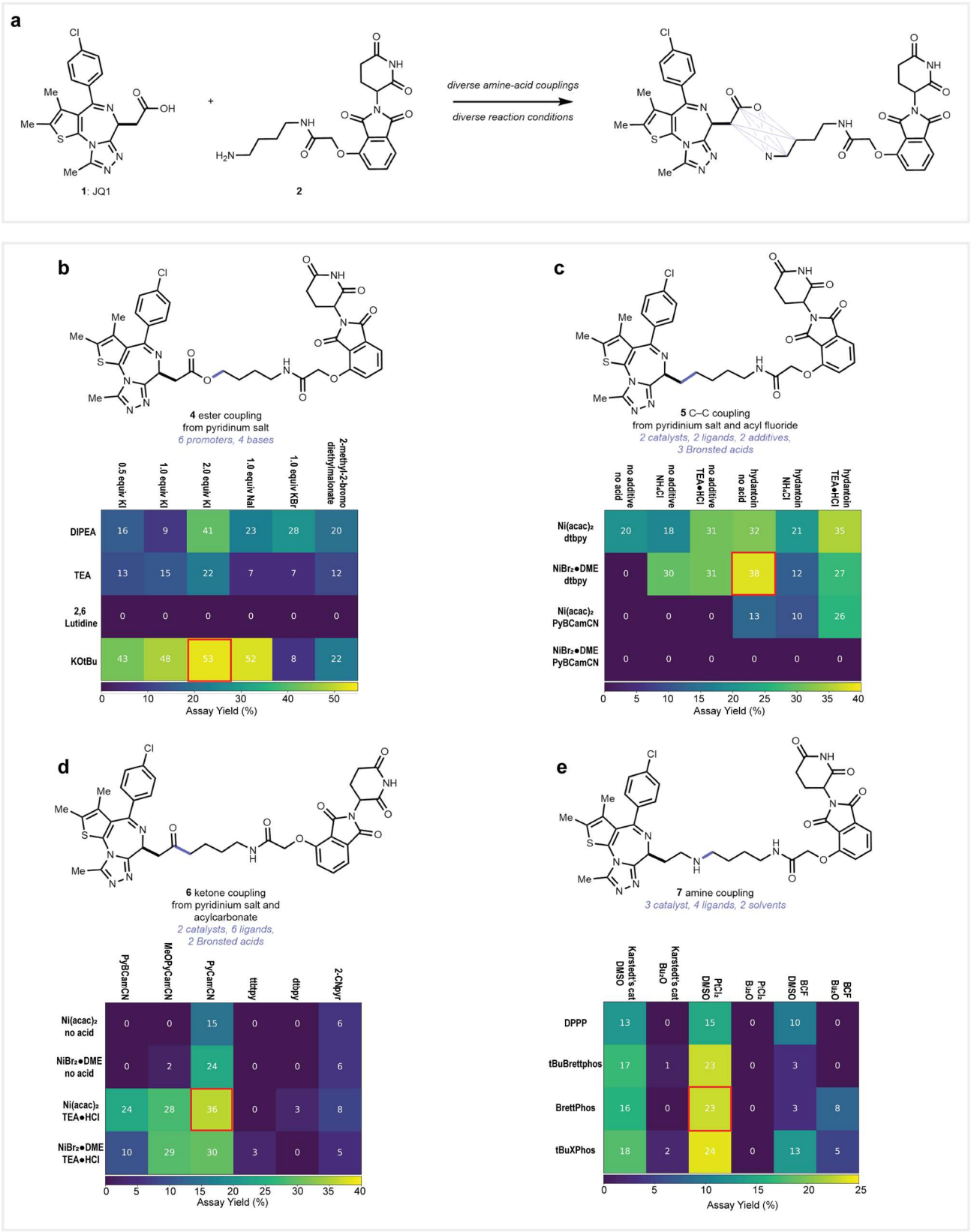

Figure 2. *(a)* Developing diverse reaction conditions to produce ester, amine, alkane, and ketone-linked analogs of amide dBET1 (3) using high-throughput experimentation. Assay yields were determined by UPLC-MS. (b) Ester array conditions: 10 μmol of **1** (1.0 equiv), **10** (1.0 equiv), base (1.0 equiv) and additive (equiv listed) per well. (c) Alkane array conditions: 5 μmol (2.0 equiv) of **8**, **10** (1.0 equiv), nickel catalyst (40 mol%), ligand (40 mol %), imide additive (2.0 equiv), Brønsted acid (2.0 equiv), and manganese (4.0 equiv) per well. (d) Ketone array conditions: 5 μmol (2.0 equiv) of **9**, (1.0 equiv), nickel catalyst (40 mol%), ligand (40 mol %), additive (2.0 equiv), and manganese (4.0 equiv) per well. (e) Amine array conditions: 15 μmol **1** (1.5 equiv), **2** (1.0 equiv), catalysts (5 mol %), ligand (10 mol %), and phenylsilane (4 equiv) per well. All wells contain 100 μL of solvent. PyBCamCN = (2*Z*,6*Z*)-N′2,N′6-Dicyanopyridine-2,6-bis(carboximidamide), MeOPyCamCN = 4-methoxy-N-cyanopicolinimidamide PyCamCN = N-cyanopicolinimidamide, ttbtpy = 4,4′,4″-Tri-tert-Butyl-2,2′:6′,2″-terpyridine**,** dtbpy = 4,4-di-tert-butylbipyridine, 2CNPyr = 2-cyanopyridine, Karstedt's cat = Platinum(0)-1,3-divinyl-1,1,3,3-tetramethyldisiloxane complex.

https://doi.org/10.26434/chemrxiv-2023-bh0d1 **ORCID:** https://orcid.org/0000-0001-9275-0017

Results and Discussion

Our studies initiated with a campaign to identify diverse reaction conditions for linking **1** and **2** that would produce PROTAC molecules **3**–**7**. We used miniaturized high throughput experimentation (HTE), which has emerged as a powerful tool in the navigation of reaction space.[25–28] In addition to allowing a rapid assessment of the interplay of multiple reaction variables, the use of miniature glass vials allows for conservation of precious starting materials,[29] such as partial PROTAC building blocks. HTE investigation of the four targeted amine–acid coupling transformations esterification, alkylation, ketonylation, or amination was conducted surveying 24 unique reaction conditions each. Reactions were performed on less than 10 μmol scale of starting material **2** per well (Figure 2a).

Automatable amine–acid esterification reactions have been developed by our lab for both alkyl[19] and aryl amines.[18] In the alkyl amine setting, the esterification proceeds via activation of the alkyl amine as its triphenylpyridinium salt[30] and aging with a carboxylic acid in the presence of *N,N*-diispropylethylamine (DIPEA) and potassium iodide (KI). When **1** and the pyridinium salt of **2** were subjected to these conditions, the desired ester was observed alongside an undesired isobaric compound presumed to be from imine N-alkylation (Supporting Information, Figure S10). Thus, a 24-well reaction array examining different promoter additives and bases was performed to identify alternative reaction conditions for the formation of desired ester **4** (Figure 2b). In general, stronger bases facilitated the formation of the desired ester product. For instance, potassium *tert*-butoxide yielded **4** as the exclusive product whereas lutidine exclusively formed the undesired adduct. DIPEA and triethylamine (TEA) gave mixtures of both the desired product and the undesired adduct. Potassium bromide (KBr) and bromomethyldiethyl malonate facilitated the reaction as additives, but in lower yield than KI or sodium iodide (NaI). The best performing conditions used KI and potassium *tert*-butoxide and gave **4** in 53% assay yield and 54% isolated yield. This protocol complements multistep synthesis methods to access ester-linked PROTACs via total synthesis.[10]

To access the alkane and ketone linked products, we explored nickel-catalyzed reductive cross-couplings conditions. Recent methods employing nickel as the metal catalyst have emerged as a powerful tool to link pyridinium salts[31–35] and activated carboxylic acids for the formation of alkanes or ketones[36–39], and we hypothesized that a reducing nickel system would best facilitate the formation of alkane (**5**) and ketone (**6**) targets. We began our investigation through coupling acyl fluoride **8** (Figure 3), generated *in-situ* from **1** using tetramethylfluoroformamidinium hexafluorophosphate (TFFH) and proton sponge, and **10** (pyridinium salt of **2**). Subjecting these coupling partners to nickel (II) bromide•glyme ($NiBr_2$•DME), 4,4-di-*tert*-butylbipyridine (dtbpy), and elemental manganese produced alkane product **5**. A thorough investigation of the interplay of imide additives (see Supporting Information)[40], nickel sources, ligands, and Brønsted acid additives (Figure 2c) was conducted. We found that hydantoin increased alkane formation whereas the inclusion of Brønsted acids was detrimental. $NiBr_2$•DME, and dtbpy were observed to be the optimal catalyst and ligand combination giving **5** in 38% assay yield.

In our investigation of ligands to synthesize alkane **5**, we observed a ligand change occasionally yielded mixtures of **5** and ketone **6** (see Supporting Information). Based on these observations we hypothesized we could access **6** through careful selection of catalyst, ligand and additive. Thorough investigation revealed we should explore other activation strategies (see Supporting Information). For substrates derived from **1**, we determined acyl carbonates to be a viable activating group.[38] Subsequently, JQ1 (**1**) was activated *in situ* by using dimethyldicarbonate (DMDC). After determining our optimal activating group, we investigated the use of imides, Brønsted acids, and ligands (Figure 2d). We found the ligand (*Z*)-*N*-cyanopicolinimidamide (PyCamCN) maximized the yield of **6,** whereas dtbpy gave alkane **5** exclusively. Notably, in contrast to our findings in the C–C coupling of **1** and **2**, the use of imide additives hindered ketone formation while triethylammonium hydrochloride (NEt_3•HCl) was found to increase the yield. We selected *in situ* activation of **1** with DMDC and catalyzed ketonylation with nickel (II) acetylacetonate $Ni(acac)_2$, PyCamCN, and NEt_3•HCl as optimal conditions to deliver **6** in 36 % assay yield.

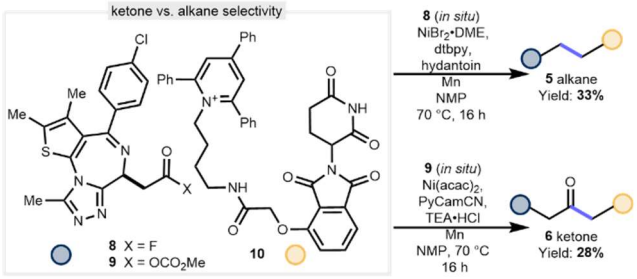

Figure 3. A change in ligand switches the selectivity for the synthesized product. Reactions conducted using **8** or **9** (2.0 equiv), **10** (1.0 equiv), nickel catalyst and ligand (40 mol % each), additive (2.0 equiv), and manganese (4.0 equiv) at 0.025 M.

We were intrigued by the rapid decarbonylation of the acyl fluoride **8** to give alkane product **5** as opposed to ketone product **6** when subjected to nickel and dtbpy, in contrast to literature reports (Figure 3).[7,36] This may be due to subtle changes in electronics of the substrate having a profound impact on the rate of decarbonylation in nickel catalyzed reactions.[21] Mechanistic investigations in our lab and others[21,37,41,42] have highlighted that subtle effects govern the decarbonylation event in nickel-catalyzed reductive cross-couplings. In addition, ligands may also play a role in governing the kinetics of decarbonylation; when the acyl carbonate of **1** and pyridinium salt of **2** were subjected to $NiBr_2$•DME and dtbpy, only the decarbonylated alkyl coupling product **5** was observed albeit in lower yield. To

further probe this effect, we investigated other amine and carboxylic acid coupling partners under our reaction conditions (see Supporting Information). In general, we have discovered that selectivity for C–C coupling is consistent in the case of primary pyridinium salts whereas only the ketone product is observed when using secondary pyridinium salts. The rapid decarbonylation is also observed in carboxylic acids containing α β-diphenyl imine group. Further investigations into this effect are ongoing in our lab.

We next turned our attention to the formal reductive amination between **1** and **2**. Based upon literature precedent[43,44], we believed the desired reactivity could be achieved using either platinum based catalysis or *tris*(pentafluorophenyl)borane (BCF). BCF in dibutylether (Bu_2O) produced a trace amount of desired amine **7** along with amide **3** and recovered starting material, and no reduction of the amide bond or four other carbonyls. Further investigation of solvent effect demonstrated that DMSO outperforms other polar aprotic solvents (see Supporting Information) suggesting that the effect is not entirely solubility driven. Based upon these data we planned a screen investigating solvents, catalysts, and ligands. Three catalysts (two platinum and BCF), and four phosphine ligands, were surveyed by HTE using DMSO or dibutyl ether as solvent. Our observations confirmed that DMSO is essential to achieving reactivity with these complex substrates, which contrasts reports on simpler substrates.[43–45] Additionally, platinum catalysis outperformed boron catalysis with platinum (II) chloride being an optimal catalyst and BrettPhos as a preferred ligand.

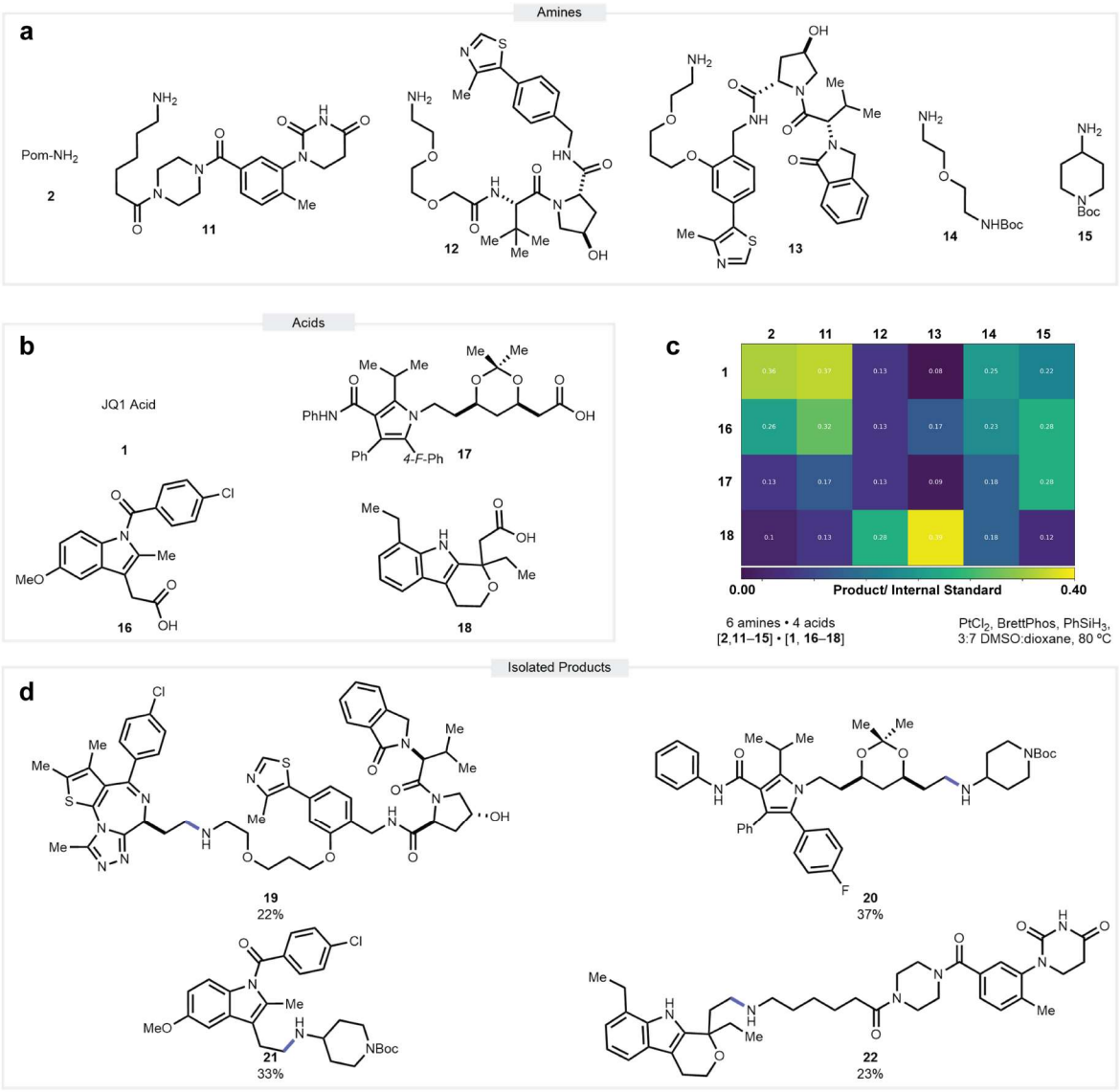

Figure 4. Reductive amination conditions applied to a library of (a) 6 amines and (b) 4 acids. All reactions conducted using 10 μmol of amine (1.0 equiv) and 15 μmol of acid (1.5 equiv), $PtCl_2$ (5 mol %), BrettPhos (10 mol %) and $PhSiH_3$ (5.0 equiv) at 0.1 M. (c) Results of the screen (d) (d) Scale up of select compounds on 0.100 mmol scale relative to the amine starting material.

To further explore the scope of the reductive amination reaction we applied our optimized condition to an array of six amines including four partial PROTACs (**2**, **11**–**13**), two linker type molecules (**14**, **15**) (Figure 4a) and four pharmaceutically relevant carboxylic acids (**1**, **16**–**18**) (Figure 4b). Since we have seen that CRBN targeting ligands such as **2** and **11** generally perform better in pure DMSO, and other systems perform better using a mixture of DMSO and dioxane, we settled on 30% DMSO in dioxane as a balance. These conditions appear broadly applicable to late-stage derivatization as we saw product formed in every well (Figure 4c). This is remarkable as the reaction performs in the presence of functionalities such as alcohols (**12**,**13**), acetonides (**17**), a dihydrouracil (**11**), and an indole (**16**). Additionally, the reaction works on aliphatic as well as benzylic acids. To assess the performance of the reaction we isolated products from four wells on a 0.1 mmol scale (**19**–**22**) (Figure 4d and 4e). In each of these reactions, we did not observe reduction of other carbonyls present in the molecule. These results as well as control experiments leaving the amine out (see Supporting Information) suggest a pathway where an aldehyde intermediate plays a dominant role as opposed to amide formation and subsequent reduction.[43,44,46] The ester, alkane, and ketone transformations as well as the amide coupling were also applied to this library (see Supporting Information).

With optimized conditions for each transformation, we turned our attention towards the scale up and isolation of each compound in practically useful amounts (0.1 mmol scale) (Figure 5a). Due to the immense interest in using VHL as an E3 ligase as a complementary approach to protein degradation, we applied our conditions to VHL targeting amine **13**.[3,4,47] We observed similar reactivity trends despite incorporating new functional groups with the potential to interfere. Scale up of our conditions was

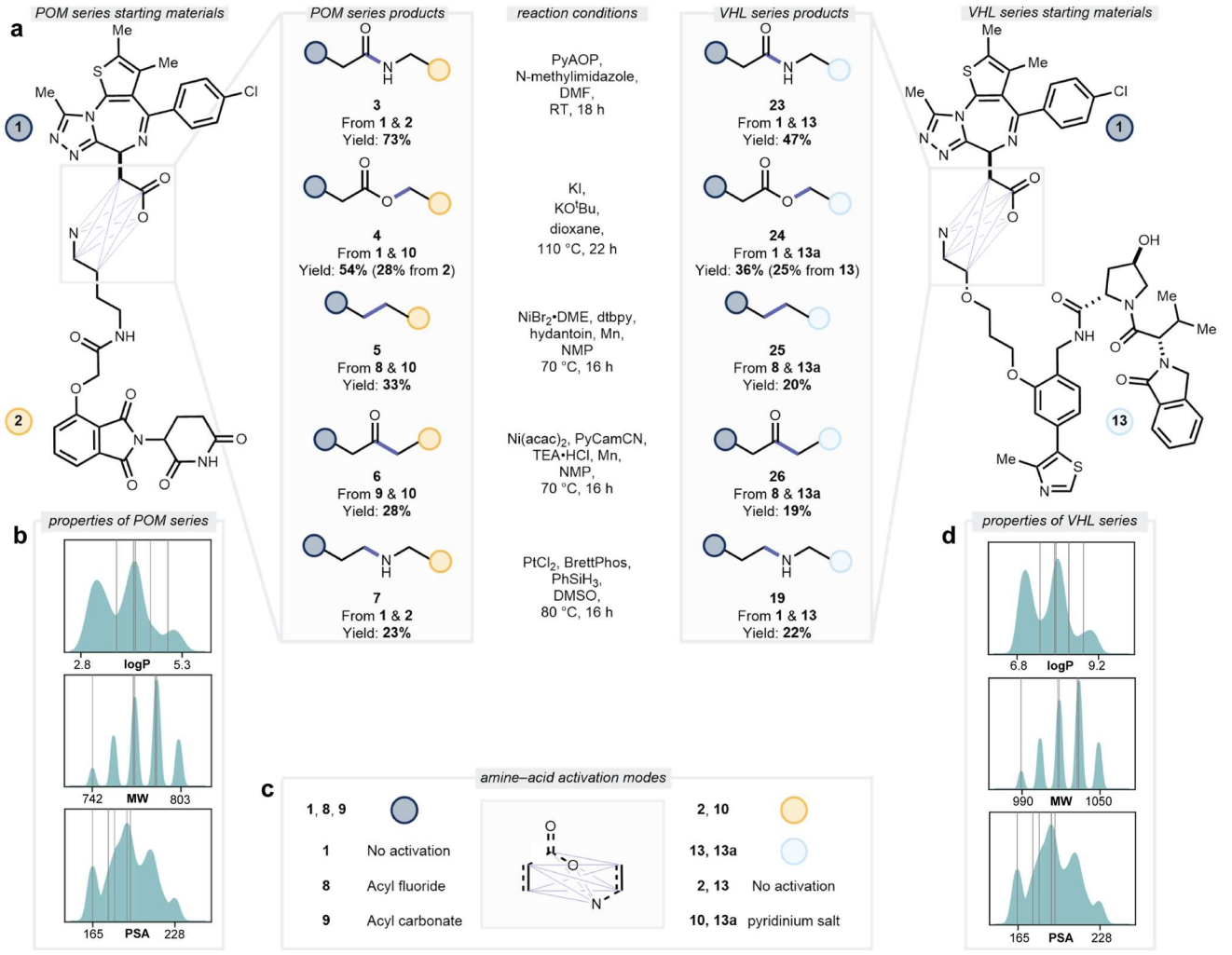

Figure 5 (a) Five transformations applied to **1** & **2** (POM), as well as **1** and **13** (VHL)**.** All reactions conducted at 0.100 mmol scale relative to the amine. Amide conditions: **1** and **2** (1.0 equiv), PyAOP (1.0 equiv), and N-methylimidazole (1.0 equiv) in 1.0 mL of solvent (0.1 M). Ester reaction conditions: **1** and **10** (1.0 equiv), KI (2.0 equiv), and KO^{t}Bu (1.0 equiv) in 1.0 mL solvent (0.1 M). CC and Ketone conditions: **1** (2.0 equiv), **2** (1.0 equiv), nickel catalyst (40 mol%), ligand (40 mol %), additive (2.0 equiv), and manganese (4.0 equiv) in 2.0 mL solvent 0.05 M. Amine conditions: **1** (1.5 equiv) and **2** (1.0 equiv) $PtCl_2$ (5 mol %), BrettPhos (10 mol %) and $PhSiH_3$ (5.0 equiv). (b) Chemoinformatic analysis of **3**-**7**. (c) methods used to activate the amine or acid coupling partner (d) Chemoinformatic analysis of **19**, **23**-**26**.

found to correlate well with assay yield for each transformation and delivered both the CRBN and VHL based PROTACs in acceptable yield. Our amide conditions (see Supporting Information) yielded compound **3** in 73% and compound **23** in 47% yields respectively. Applying our esterification conditions to each substrate yielded ester **4** in 54% and ester **24** in 36% yields. Further, a one-pot protocol (see Supporting Information) was developed to give **4** directly from **1** and **2** in 28% yield. A slightly modified protocol using two equivalents of base was applied to the HCl salt **13** to give **24** in 25% yield. Applying our alkane conditions yielded **5** in 33% and **25** in 20% yields respectively. Application of our ketone conditions yielded **6** and **26** in 28% and 19% yields. Finally, our conditions for reductive amination yielded **7** in 23% yield. It was found it was necessary to adjust the solvent to 10% DMSO in dioxane to achieve optimal reactivity for the synthesis of **19**. This adjustment furnished **19** in 23% yield. It is of note that we did not observe opening of the glutarimide ring under any of our reaction conditions.[48,49] With nine new dBET1 analogs in hand, calculations were performed on each molecule to demonstrate that we can effectively modulate the properties of each final PROTAC by changes to the linker composition (Figure 5b, 5d). While bulk properties are determined by choice of building blocks (**2** vs **13**), each transformation imparts its own effect on the overall properties of the molecule with removal of the hydrogen bond donor (amide/amine to ester/alkane/ketone) having the greatest impact in this investigation (see Supporting Information for labels).

Having established conditions to scale up and isolate the 10 BRD4 PROTACs (**3–7**, **19**, **23–26**), in vitro profiling in our primary biological assays to assess BRD4 degradation was initiated. We tested both CRBN-based PROTACs **3–7** as well as VHL (**19**, **23–26**) using HEK293 cells to readout endogenous BRD4 degradation DC_{50} and D_{max} values.[50] In addition, to separate on target BRD4 degradation from general cell toxicity, Cell Titer Glo (CTG) was also conducted (see Supporting Information). Within the CRBN-BRD4 PROTAC series, we observed several molecules with more efficient BRD4 degradation than dBET1 (**3**) (Figure 6). The ester **4**, alkane **5** and ketone **6** were more potent than amide **3**, with DC_{50} values of 5.4 nM, 10.8 nM, 9.2 nM, and 95.0 nM, respectively. Comparable target degradation to amide **3** (D_{max} 80%), was observed for **4**, **5**, and **6** (83%, 76% and 85% at 24 h). Conversely, the amine analog **7** was not successful at degrading BRD4 with a DC_{50} of > 11 µM. In general, the VHL-based PROTACs **19**, **23–26**, follow the same trend in BRD4 degradation as observed for the four linkages compared to the CRBN series (see Figure 6b), albeit DC_{50} values are higher and D_{max} values lower. VHL ester **24** and ketone **26** are the most efficient degraders of BRD4 in the set, with DC_{50} values of 27.3 nM and 13.4 nM (D_{max} values of 80% and 79%, respectively). VHL alkane **25** has a 21-fold higher DC_{50} and diminished D_{max} value relative to CRBN alkane **5**, likely due to reduced binding to BRD4 and VHL protein (see Table S20 in Supporting Information).

To understand the observed BRD4 degradation results that arose from subtle changes to the linker, we

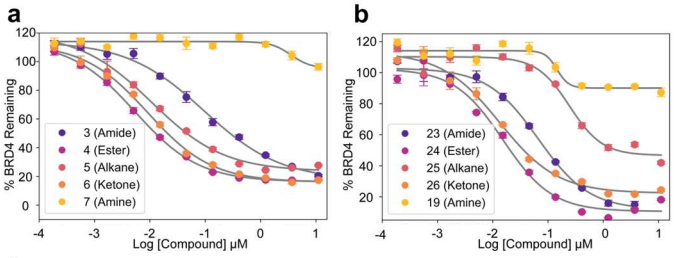

c

E3 Ligase	Linker Type (#)	MW	CHI $LogD_{7.4}$	BRD4 HTRF degradation DC_{50} (nM)	BRD4 HTRF degradation D_{max} (%)
CRBN	amide (**3**)	785	2.16	95.0 ± 7.2	80
CRBN	ester (**4**)	786	2.68	5.4± 1.0	83
CRBN	alkane (**5**)	742	2.81	10.8 ± 0.9	76
CRBN	ketone (**6**)	770	2.57	9.2 ± 1.0	85
CRBN	amine (**7**)	771	1.66	>11,000	2
VHL	amide (**23**)	1033	2.78	68.3 ± 6	87
VHL	ester (**24**)	1034	3.25	15.8 ± 1.5	89
VHL	alkane (**25**)	990	3.38	228.0 ± 16.7	58
VHL	ketone (**26**)	1018	3.16	13.4 ± 0.9	79
VHL	amine (**19**)	771	2.30	11,000	14

Figure 6 BRD4 HTRF Degradation Assay: (a) CRBN series degradation curves (3-7). (b) VHL series degradation curves (19, 23-26). (c) Table 1. Table of experimental physicochemical properties and BRD4 HTRF degradation values. Values reported are the mean ± SEM of a single experiment in quadruplicate.

measured target engagement of the heterobifunctional degraders to BRD4 protein and the corresponding E3 ligase (Table 2). Binding affinity of the PROTACs to BRD4 **3–7** was assessed in a BRD4-BD1 biochemical probe displacement assay to bromodomain BD1. E3 ligase engagement was evaluated in a cellular CRBN or VHL nanoBRET (Bioluminescence Resonance Energy Transfer) assay dependent on the PROTAC synthesized. The cellular nanoBRET target engagement assay was used as a surrogate to examine PROTAC cellular permeability.[51] The assay was performed in both live and permeabilized (lytic) cells and intracellular

Linker Type (#)	BRD4-BD1 HTRF (nM)	nanoBRET Live (nM)	nanoBRET Permeabilized (nM)	nanoBRET RBA
amide (**3**)	16.0 ± 1.1	528.5 ± 35.0	86.3 ± 4.8	6.1
ester (**4**)	2.3 ± 0.1	263.7 ± 7.6	68.8 ± 4.4	2.4
alkane (**5**)	66.9 ± 1.1	503.5 ± 19.9	120.7 ± 14.2	4.2
ketone (**6**)	24.2 ± 0.9	421.8 ± 21.1	107.1 ± 15.9	3.9
amine (**7**)	453.2 ± 18.4	11272 ± 1992.7	102.0 ± 4.9	110.5

Table 2 Target engagement for CRBN analogs (3-7) assessed by BRD4-BD1 HTRF displacement assay and cellular nanoBRET CRBN-tracer assay in live and permeabilized conditions. Values reported are the mean ± SEM of a single experiment in triplicate for the BRD4—BD1 HTRF assay . Values reported are the mean ± SEM of a single experiment containing five technical replicates for the celullar nanoBRET CRBN-tracer assay.

availability was determined by calculating the relative binding affinity (RBA).[52]

Table 2 shows the data for the five CRBN-BRD4 PROTACs using amide **3** as a benchmark, which has a BRD4 affinity of 16.0 nM, and CRBN binding of 528.5 nM (live cells) and 86.3 nM (permeabilized cells). Of the newly synthesized analogs, ester **4**, alkane **5**, and ketone **6** maintain binding with IC_{50} values of 2.2, 66.9, and 24.2 nM for BRD4, respectively. Notably removal of the carbonyl moiety in alkane **5** does not result in a significant loss in BRD4 affinity (Table 2). Looking at the RBA values, a decrease is seen for ester **4**, alkane **5**, and ketone **6**, (RBA: 2.4, 4.2, and 3.9, respectively, relative to **3**). This is possibly because these three analogs have higher LogD, correlating with an anticipated increase in permeability. All three of these analogs have the HBD N–H group seen in amide **3** removed. The SAR trend observed for BRD4 degradation has **4**–**6** as the most potent degraders and the improvement in permeability and BRD4 affinity may be an explanation for the observed degradation. VHL degraders **19**, **23**–**26** occupy less drug-like space due to their higher molecular weight and larger number of HBD but still show the same rank order in BRD4 target engagement and improved RBA values (see Supporting information). However, the lower VHL affinity in live cell nanoBRET for **19**, **23**–**26** may explain the rightward shift in DC_{50} values (Figure 6, Table 1). High degradation efficacy of BRD4 is retained by VHL PROTACs with D_{max} ranging from 58–83%. Amine **7** shows a greater than 100-fold difference in IC_{50} between the live and permeabilized cells and this can be attributed to the presence of the basic amine in the linker. Additionally, the BRD4 potency of amine **7** is 453 nM compared to 15 nM for amide **3**. Further investigation of this significant shift in potency to the protein of interest was investigated computationally.

To understand the differences in binding affinity of highly potent versus poor binders, molecular dynamic simulations of BRD4-BD1 in the presence of amide **3**, ester **4**, and amine **7** were conducted in explicit solvent conditions. Sampled conformations from the 250-ns MD simulations are shown in Figure 8 (initial pose is shown in red and final in blue). Based on the simulations, both amide **3** and ester **4** maintains key interactions with the BRD4 binding site. In contrast, amine **7** due to presence of a charged linker, interacts with Asp144 and engages in an intramolecular hydrogen bond with the azepine moiety on the POI portion during the course of the simulation (see Supporting Information for 2D interaction diagram). These observed interactions significantly alter the conformation of amine **7** as seen during MD simulation (Figure 8). Furthermore, the BRD4-BD1 protein near the binding region of the amine **7** displays significantly higher root-mean-square fluctuation (RMSF) compared to amide **3** or ester **7** compounds. This instability of the amine **7** interaction with BRD4 along with conformational preference could influence productive ternary

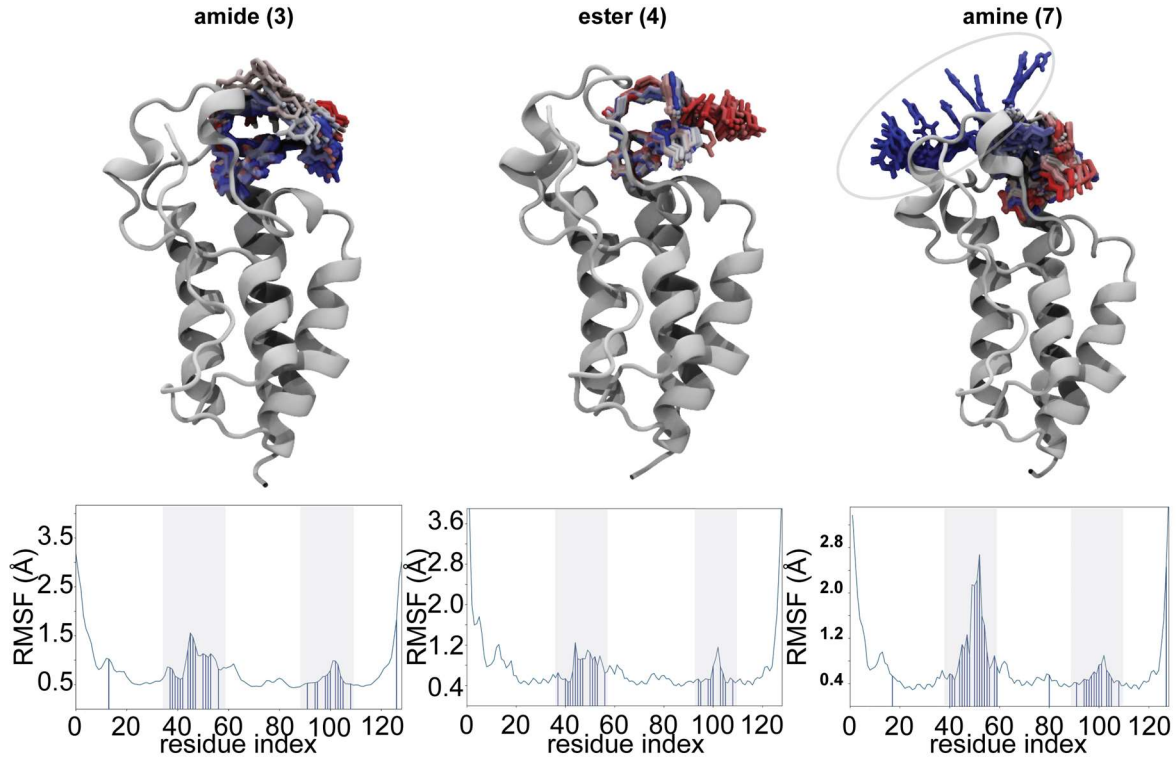

Figure 8. Molecular dynamic simulations of PROTACs 3, 4, and 7 bound to the BRD4-BD1 crystal structure. Time-lapse snapshots from 250-ns simulations are shown overlaid and depicted using color changes from red to blue indicating initial to final binding pose.

complex formation and contribute to the lower observed degradation.

In conclusion, by harnessing the power of HTE we have developed four unique transformations, esterification, alkylation, ketonylation, and amination to quickly access a suite of BRD4 degraders with modifications to the linker. Importantly these adjustments to the linker connectivity have been achieved using JQ-1 as the target binding moiety and several types of E3 ligase recruiters. The ester, ketone, and alkane transformations all removed the HBD moiety imparted by the amide transformation, leading to higher LogD values, and increased cellular permeability. This is contrasted by the amine, which retains the hydrogen bond donor and has a significantly lower LogD due to its charge and is less permeable. The structural changes also affect binding with removal of the carbonyl having the largest effect. Computational studies indicate this change is not tolerated in amine **7**. These combined effects led to more potent degraders when the amide is exchanged for an ester, alkane, or ketone, but ineffective degraders when exchanged for an amine. Given the impact new transformations have on the properties and of PROTACs, there is a need to develop new amine–acid couplings that perform on densely functionalized PROTACs.

ASSOCIATED CONTENT

Supporting Information

Data Availability Statement Code used to generate the tSNE as well as the potency graphics, SMILES strings of all enumerated products, and an interactive version of the tSNE are available at https://github.com/cernak-lab/cernak-lab.github.io/tree/main/publications/McGrath%20Diverse%20Amine-Acid%20Couplings%20PROTACs

AUTHOR INFORMATION

Corresponding Authors

***Tim Cernak–Department of Medicinal Chemistry, College of Pharmacy, University of Michigan, Ann Arbor, Michigan 48109, United States; Department of Chemistry, University of Michigan, Ann Arbor, Michigan 48109, United States; orcid.org/0000-0001-5407-0643**

Email: tcernak@med.umich.edu

***Christine Gelin - Discovery Chemistry, Therapeutics Discovery, Janssen Research & Development, LLC, 3210 Merryfield Row, La Jolla, California 92121, United States orcid.org/**

Email: cgelin@its.jnj.com

Present Addresses

Andrew McGrath - Department of Medicinal Chemistry, College of Pharmacy, University of Michigan, Ann Arbor, Michigan 48109, United States: https://orcid.org/0000-0001-9275-0017

Haiyan Huang - Department of Medicinal Chemistry, College of Pharmacy, University of Michigan, Ann Arbor, Michigan 48109, United States: https://orcid.org/ 0009-0005-9761-8441

Jean-Francois Brazeau - Discovery Chemistry, Therapeutics Discovery, Janssen Research & Development, LLC, 3210 Merryfield Row, La Jolla, California 92121, United States: https://orcid.org/0009-0000-4568-3923

Zirong Zhang† – Oncology Research and Development, AstraZeneca, Waltham, Massachusetts, 02451, United States: https://orcid.org/0000-0002-6720-4644

Lu Zhu - Discovery Technologies & Molecular Pharmacology, Therapeutics Discovery, Janssen Research & Development, LLC, Welsh & McKean Roads, Spring House, Pennsylvania 19477, United States: https://orcid.org/0000-0001-9438-9296

Zhicai Shi - Discovery Chemistry, Therapeutics Discovery, Janssen Research & Development, LLC, Welsh & McKean Roads, Spring House, Pennsylvania 19477, United States

Jennifer Venable - Discovery Chemistry, Therapeutics Discovery, Janssen Research & Development, LLC, 3210 Merryfield Row, La Jolla, California 92121, United States

Author Contributions

The manuscript was written through contributions of all authors.

Funding Sources

This work was funded by Janssen Therapeutics, and NIH-R01GM144471 (TC). Notes: The authors declare the following competing financial interest(s): The Cernak Lab has received research funding or in-kind donations from MilliporeSigma, Relay Therapeutics, Janssen Therapeutics, SPT Labtech,Entos, Inc. and Merck & Co., Inc. T.C. holds equity in Scorpion Therapeutics and is a co-Founder and equity holder of Entos, Inc.

ACKNOWLEDGMENT

We would like to thank Paige Stout and Marcus Gutierrez for purification (reverse phase HPLC) of select compounds and Deszra Shariff for NMR analysis of select compounds. We thank Charu Chaudhry for helpful discussions during the preparation of the manuscript.

REFERENCES

(1) Cyrus, K.; Wehenkel, M.; Choi, E.-Y.; Han, H.-J.; Lee, H.; Swanson, H.; Kim, K.-B. Impact of Linker Length on the Activity of PROTACs. *Mol. Biosyst.* **2011**, *7* (2), 359–364. https://doi.org/10.1039/C0MB00074D.

(2) Bashore, F. M.; Foley, C. A.; Ong, H. W.; Rectenwald, J. M.; Hanley, R. P.; Norris-Drouin, J. L.; Cholensky, S. H.; Mills, C. A.; Pearce, K. H.; Herring, L. E.; Kireev, D.; Frye, S. V.; James, L. I. PROTAC Linkerology Leads to an Optimized Bivalent Chemical Degrader of Polycomb Repressive Complex 2 (PRC2) Components. *ACS Chem. Biol.* **2023**, *18* (3), 494–507. https://doi.org/10.1021/acschembio.2c00804.

(3) Zoppi, V.; Hughes, S. J.; Maniaci, C.; Testa, A.; Gmaschitz, T.; Wieshofer, C.; Koegl, M.; Riching, K. M.; Daniels, D. L.; Spallarossa, A.; Ciulli, A. Iterative Design and Optimization of Initially Inactive Proteolysis Targeting Chimeras (PROTACs) Identify VZ185 as a Potent, Fast, and Selective von Hippel–Lindau (VHL) Based Dual Degrader Probe of BRD9 and BRD7. *J. Med. Chem.* **2019**, *62* (2), 699–726. https://doi.org/10.1021/acs.jmedchem.8b01413.

(4) Hu, J.; Hu, B.; Wang, M.; Xu, F.; Miao, B.; Yang, C.-Y.; Wang, M.; Liu, Z.; Hayes, D. F.; Chinnaswamy, K.; Delproposto, J.; Stuckey, J.; Wang, S. Discovery of ERD-308 as a Highly Potent Proteolysis Targeting Chimera (PROTAC) Degrader of Estrogen Receptor (ER). *J. Med. Chem.* **2019**, *62* (3), 1420–1442. https://doi.org/10.1021/acs.jmedchem.8b01572.

(5) Li, M.; Zhi, Y.; Liu, B.; Yao, Q. Advancing Strategies for Proteolysis-Targeting Chimera Design. *J. Med. Chem.* **2023**, *66* (4), 2308–2329. https://doi.org/10.1021/acs.jmedchem.2c01555.

(6) Maple, H. J.; Clayden, N.; Baron, A.; Stacey, C.; Felix, R. Developing Degraders: Principles and Perspectives on Design and Chemical Space. *MedChemComm* **2019**, *10* (10), 1755–1764. https://doi.org/10.1039/C9MD00272C.

(7) Békés, M.; Langley, D. R.; Crews, C. M. PROTAC Targeted Protein Degraders: The Past Is Prologue. *Nat. Rev. Drug Discov.* **2022**, *21* (3), 181–200. https://doi.org/10.1038/s41573-021-00371-6.

(8) Papatzimas, J. W. ; G., Evgueni; Brownsey, Duncan K. ;. Maity, Ranjan; Bahlis, Nizar J. ;. Derksen, Darren J. A General Strategy for the Preparation of Thalidomide-Conjugate Linkers. *Synlett* **2017**, *28* (20), 2881–2885. https://doi.org/10.1055/s-0036-1588539.

(9) Bhela, I. P.; Ranza, A.; Balestrero, F. C.; Serafini, M.; Aprile, S.; Di Martino, R. M. C.; Condorelli, F.; Pirali, T. A Versatile and Sustainable Multicomponent Platform for the Synthesis of Protein Degraders: Proof-of-Concept Application to BRD4-Degrading PROTACs. *J. Med. Chem.* **2022**, *65* (22), 15282–15299. https://doi.org/10.1021/acs.jmedchem.2c01218.

(10) Klein, V. G.; Bond, A. G.; Craigon, C.; Lokey, R. S.; Ciulli, A. Amide-to-Ester Substitution as a Strategy for Optimizing PROTAC Permeability and Cellular Activity. *J. Med. Chem.* **2021**, *64* (24), 18082–18101. https://doi.org/10.1021/acs.jmedchem.1c01496.

(11) Wurz, R. P.; Dellamaggiore, K.; Dou, H.; Javier, N.; Lo, M.-C.; McCarter, J. D.; Mohl, D.; Sastri, C.; Lipford, J. R.; Cee, V. J. A "Click Chemistry Platform" for the Rapid Synthesis of Bispecific Molecules for Inducing Protein Degradation. *J. Med. Chem.* **2018**, *61* (2), 453–461. https://doi.org/10.1021/acs.jmedchem.6b01781.

(12) Brownsey, D. K.; Rowley, B. C.; Gorobets, E.; Gelfand, B. S.; Derksen, D. J. Rapid Synthesis of Pomalidomide-Conjugates for the Development of Protein Degrader Libraries. *Chem. Sci.* **2021**, *12* (12), 4519–4525. https://doi.org/10.1039/D0SC05442A.

(13) Hayhow, T. G.; Borrows, R. E. A.; Diène, C. R.; Fairley, G.; Fallan, C.; Fillery, S. M.; Scott, J. S.; Watson, D. W. A Buchwald–Hartwig Protocol to Enable Rapid Linker Exploration of Cereblon E3-Ligase PROTACs**. *Chem. – Eur. J.* **2020**, *26* (70), 16818–16823. https://doi.org/10.1002/chem.202003137.

(14) Guo, L.; Zhou, Y.; Nie, X.; Zhang, Z.; Zhang, Z.; Li, C.; Wang, T.; Tang, W. A Platform for the Rapid Synthesis of Proteolysis Targeting Chimeras (Rapid-TAC) under Miniaturized Conditions. *Eur. J. Med. Chem.* **2022**, *236*, 114317. https://doi.org/10.1016/j.ejmech.2022.114317.

(15) Qiu, X.; Sun, N.; Kong, Y.; Li, Y.; Yang, X.; Jiang, B. Chemoselective Synthesis of Lenalidomide-Based PROTAC Library Using Alkylation Reaction. *Org. Lett.* **2019**, *21* (10), 3838–3841. https://doi.org/10.1021/acs.orglett.9b01326.

(16) Mahjour, B.; Shen, Y.; Liu, W.; Cernak, T. A Map of the Amine–Carboxylic Acid Coupling System. *Nature* **2020**, *580* (7801), 71–75. https://doi.org/10.1038/s41586-020-2142-y.

(17) Zhang, R.; Mahjour, B.; Cernak, T. Exploring the Combinatorial Explosion of Amine–Acid Reaction Space via Graph Editing. *ChemRxiv* **2022**. https://doi.org/10.26434/chemrxiv-2022-917k5.

(18) Shen, Y.; Mahjour, B.; Cernak, T. Development of Copper-Catalyzed Deaminative Esterification Using High-Throughput Experimentation. *Commun. Chem.* **2022**, *5* (1), 83. https://doi.org/10.1038/s42004-022-00698-0.

(19) McGrath, A.; Zhang, R.; Shafiq, K.; Cernak, T. Repurposing Amine and Carboxylic Acid Building Blocks with an Automatable Esterification Reaction. *Chem. Commun.* **2023**, *59* (8), 1026–1029. https://doi.org/10.1039/D2CC05670D.

(20) Zhang, Z.; Cernak, T. The Formal Cross-Coupling of Amines and Carboxylic Acids to Form Sp3–Sp3 Carbon–Carbon Bonds. *Angew. Chem. Int. Ed.* **2021**, *60* (52), 27293–27298. https://doi.org/10.1002/anie.202112454.

(21) Douthwaite, J. L.; Zhao, R.; Shim, E.; Mahjour, B.; Zimmerman, P. M.; Cernak, T. Formal Cross-Coupling of Amines and Carboxylic Acids to Form Sp3–Sp2 Carbon–Carbon Bonds. *J. Am. Chem. Soc.* **2023**, *145* (20), 10930–10937. https://doi.org/10.1021/jacs.2c11563.

(22) Hendrick, C. E.; Jorgensen, J. R.; Chaudhry, C.; Strambeanu, I. I.; Brazeau, J.-F.; Schiffer, J.; Shi, Z.; Venable, J. D.; Wolkenberg, S. E. Direct-to-Biology Accelerates PROTAC Synthesis and the Evaluation of Linker Effects on Permeability and Degradation. *ACS Med. Chem. Lett.* **2022**, *13* (7), 1182–1190. https://doi.org/10.1021/acsmedchemlett.2c00124.

(23) Boström, J.; Brown, D. G.; Young, R. J.; Keserü, G. M. Expanding the Medicinal Chemistry Synthetic Toolbox. *Nat. Rev. Drug Discov.* **2018**, *17* (10), 709–727. https://doi.org/10.1038/nrd.2018.116.

(24) Winter, G. E.; Buckley, D. L.; Paulk, J.; Roberts, J. M.; Souza, A.; Dhe-Paganon, S.; Bradner, J. E. Phthalimide Conjugation as a Strategy for in Vivo Target Protein Degradation. *Science* **2015**, *348* (6241), 1376–1381. https://doi.org/10.1126/science.aab1433.

(25) Mahjour, B.; Shen, Y.; Cernak, T. Ultrahigh-Throughput Experimentation for Information-Rich Chemical Synthesis. *Acc. Chem. Res.* **2021**, *54* (10), 2337–2346. https://doi.org/10.1021/acs.accounts.1c00119.

(26) Shen, Y.; Borowski, J. E.; Hardy, M. A.; Sarpong, R.; Doyle, A. G.; Cernak, T. Automation and Computer-Assisted Planning for Chemical Synthesis. *Nat. Rev. Methods Primer* **2021**, *1* (1), 23. https://doi.org/10.1038/s43586-021-00022-5.

(27) Mahjour, B.; Zhang, R.; Shen, Y.; McGrath, A.; Zhao, R.; Mohamed, O. G.; Lin, Y.; Zhang, Z.; Douthwaite, J. L.; Tripathi, A.; Cernak, T. Rapid Planning and Analysis of High-Throughput Experiment Arrays for Reaction Discovery. *Nat. Commun.* **2023**, *14* (1), 3924. https://doi.org/10.1038/s41467-023-39531-0.

(28) Mahjour, B.; Hoffstadt, J.; Cernak, T. Designing Chemical Reaction Arrays Using Phactor and ChatGPT. *Org. Process Res. Dev.* **2023**, *27* (8), 1510–1516. https://doi.org/10.1021/acs.oprd.3c00186.

(29) Wong, H.; Cernak, T. Reaction Miniaturization in Eco-Friendly Solvents. *Pharm. Green Process. Technol.* **2018**, *11*, 91–98. https://doi.org/10.1016/j.cogsc.2018.06.001.

(30) Gruntz, U.; Katritzky, A. R.; Kenny, D. H.; Rezende, M. C.; Sheikh, H. Pyridines as Leaving Groups in Synthetic Transformations: Conversion of Amines into Esters. *J. Chem. Soc. Chem.*

Commun. **1977**, No. 20, 701–701. https://doi.org/10.1039/C39770000701.

(31) Ni, S.; Li, C.-X.; Mao, Y.; Han, J.; Wang, Y.; Yan, H.; Pan, Y. Ni-Catalyzed Deaminative Cross-Electrophile Coupling of Katritzky Salts with Halides via C—N Bond Activation. *Sci. Adv.* **2019**, *5* (6), eaaw9516–eaaw9516. https://doi.org/10.1126/sciadv.aaw9516.

(32) Yi, J.; Badir, S. O.; Kammer, L. M.; Ribagorda, M.; Molander, G. A. Deaminative Reductive Arylation Enabled by Nickel/Photoredox Dual Catalysis. *Org. Lett.* **2019**, *21* (9), 3346–3351. https://doi.org/10.1021/acs.orglett.9b01097.

(33) Yue, H.; Zhu, C.; Shen, L.; Geng, Q.; Hock, K. J.; Yuan, T.; Cavallo, L.; Rueping, M. Nickel-Catalyzed C–N Bond Activation: Activated Primary Amines as Alkylating Reagents in Reductive Cross-Coupling. *Chem. Sci.* **2019**, *10* (16), 4430–4435. https://doi.org/10.1039/C9SC00783K.

(34) Liao, J.; Basch, C. H.; Hoerrner, M. E.; Talley, M. R.; Boscoe, B. P.; Tucker, J. W.; Garnsey, M. R.; Watson, M. P. Deaminative Reductive Cross-Electrophile Couplings of Alkylpyridinium Salts and Aryl Bromides. *Org. Lett.* **2019**, *21* (8), 2941–2946. https://doi.org/10.1021/acs.orglett.9b01014.

(35) Martin-Montero, R.; Yatham, V. R.; Yin, H.; Davies, J.; Martin, R. Ni-Catalyzed Reductive Deaminative Arylation at Sp3 Carbon Centers. *Org. Lett.* **2019**, *21* (8), 2947–2951. https://doi.org/10.1021/acs.orglett.9b01016.

(36) Wang, J.; Hoerrner, M. E.; Watson, M. P.; Weix, D. J. Nickel-Catalyzed Synthesis of Dialkyl Ketones from the Coupling of N-Alkyl Pyridinium Salts with Activated Carboxylic Acids. *Angew. Chem. Int. Ed.* **2020**, *59*, 13484. https://doi.org/10.1002/anie.202002271.

(37) Wang, J.; Ehehalt, L. E.; Huang, Z.; Beleh, O. M.; Guzei, I. A.; Weix, D. J. Formation of C(Sp2)–C(Sp3) Bonds Instead of Amide C–N Bonds from Carboxylic Acid and Amine Substrate Pools by Decarbonylative Cross-Electrophile Coupling. *J. Am. Chem. Soc.* **2023**. https://doi.org/10.1021/jacs.2c11552.

(38) Amani, J.; Molander, G. A. Direct Conversion of Carboxylic Acids to Alkyl Ketones. *Org. Lett.* **2017**, *19* (13), 3612–3615. https://doi.org/10.1021/acs.orglett.7b01588.

(39) Cornella, J.; Edwards, J. T.; Qin, T.; Kawamura, S.; Wang, J.; Pan, C.-M.; Gianatassio, R.; Schmidt, M.; Eastgate, M. D.; Baran, P. S. Practical Ni-Catalyzed Aryl–Alkyl Cross-Coupling of Secondary Redox-Active Esters. *J. Am. Chem. Soc.* **2016**, *138* (7), 2174–2177. https://doi.org/10.1021/jacs.6b00250.

(40) Prieto Kullmer, C. N.; Kautzky, J. A.; Krska, S. W.; Nowak, T.; Dreher, S. D.; MacMillan, D. W. C. Accelerating Reaction Generality and Mechanistic Insight through Additive Mapping. *Science* **2022**, *376* (6592), 532–539. https://doi.org/10.1126/science.abn1885.

(41) Malapit, C. A.; Bour, J. R.; Brigham, C. E.; Sanford, M. S. Base-Free Nickel-Catalysed Decarbonylative Suzuki–Miyaura Coupling of Acid Fluorides. *Nature* **2018**, *563* (7729), 100–104. https://doi.org/10.1038/s41586-018-0628-7.

(42) Fehér, P. P.; Stirling, A. Theoretical Study on the Formation of Ni(PR3)(Aryl)F Complexes Observed in Ni-Catalyzed Decarbonylative C–C Coupling of Acyl Fluorides. *Organometallics* **2020**, *39* (14), 2774–2783. https://doi.org/10.1021/acs.organomet.0c00387.

(43) Fu, M.-C.; Shang, R.; Cheng, W.-M.; Fu, Y. Boron-Catalyzed N-Alkylation of Amines Using Carboxylic Acids. *Angew. Chem. Int. Ed.* **2015**, *54* (31), 9042–9046. https://doi.org/10.1002/anie.201503879.

(44) Sorribes, I.; Junge, K.; Beller, M. Direct Catalytic N-Alkylation of Amines with Carboxylic Acids. *J. Am. Chem. Soc.* **2014**, *136* (40), 14314–14319. https://doi.org/10.1021/ja5093612.

(45) Stoll, E. L.; Tongue, T.; Andrews, K. G.; Valette, D.; Hirst, D. J.; Denton, R. M. A Practical Catalytic Reductive Amination of Carboxylic Acids. *Chem. Sci.* **2020**, *11* (35), 9494–9500. https://doi.org/10.1039/D0SC02271C.

(46) Zhang, Q.; Fu, M.-C.; Yu, H.-Z.; Fu, Y. Mechanism of Boron-Catalyzed N-Alkylation of Amines with Carboxylic Acids. *J. Org. Chem.* **2016**, *81* (15), 6235–6243. https://doi.org/10.1021/acs.joc.6b00778.

(47) Zengerle, M.; Chan, K.-H.; Ciulli, A. Selective Small Molecule Induced Degradation of the BET Bromodomain Protein BRD4. *ACS Chem. Biol.* **2015**, *10* (8), 1770–1777. https://doi.org/10.1021/acschembio.5b00216.

(48) Jarusiewicz, J. A.; Yoshimura, S.; Mayasundari, A.; Actis, M.; Aggarwal, A.; McGowan, K.; Yang, L.; Li, Y.; Fu, X.; Mishra, V.; Heath, R.; Narina, S.; Pruett-Miller, S. M.; Nishiguchi, G.; Yang, J. J.; Rankovic, Z. Phenyl Dihydrouracil: An Alternative Cereblon Binder for PROTAC Design. *ACS Med. Chem. Lett.* **2023**, *14* (2), 141–145. https://doi.org/10.1021/acsmedchemlett.2c00436.

(49) Min, J.; Mayasundari, A.; Keramatnia, F.; Jonchere, B.; Yang, S. W.; Jarusiewicz, J.; Actis, M.; Das, S.; Young, B.; Slavish, J.; Yang, L.; Li, Y.; Fu, X.; Garrett, S. H.; Yun, M.-K.; Li, Z.; Nithianantham, S.; Chai, S.; Chen, T.; Shelat, A.; Lee, R. E.; Nishiguchi, G.; White, S. W.; Roussel, M. F.; Potts, P. R.; Fischer, M.; Rankovic, Z. Phenyl-Glutarimides: Alternative Cereblon Binders for the Design of PROTACs. *Angew. Chem. Int. Ed.* **2021**, *60* (51), 26663–26670. https://doi.org/10.1002/anie.202108848.

(50) Riching, K. M.; Mahan, S.; Corona, C. R.; McDougall, M.; Vasta, J. D.; Robers, M. B.; Urh, M.; Daniels, D. L. Quantitative Live-Cell Kinetic Degradation and Mechanistic Profiling of PROTAC Mode of Action. *ACS Chem. Biol.* **2018**, *13* (9), 2758–2770. https://doi.org/10.1021/acschembio.8b00692.

(51) Vasta, J. D.; Corona, C. R.; Robers, M. B. A High-Throughput Method to Prioritize PROTAC Intracellular Target Engagement Target Engagement and Cell PermeabilityPermeability Using NanoBRETNanoBRET. In *Targeted Protein Degradation: Methods and Protocols*; Cacace, A. M., Hickey, C. M., Békés, M., Eds.; Springer US: New York, NY, 2021; pp 265–282. https://doi.org/10.1007/978-1-0716-1665-9_14.

(52) RBA Is Defined as the Ratio of a Compound's Affinity in Live versus Permeabilized Cells. A Larger Right Shift in Measured Affinity in the Live-Cell Mode Leads to Larger RBA Values and Is an Indication of Lower Permeability.